J Neuropathol Exp Neurol
Vol. 73, No. 7
July 2014
pp. 714–728

ORIGINAL ARTICLE

OPEN

Immunostaining of Oxidized DJ-1 in Human and Mouse Brains

Yoshiro Saito, PhD, Tomohiro Miyasaka, PhD, Hiroyuki Hatsuta, MD, Kazuko Takahashi-Niki, PhD, Kojiro Hayashi, Msc, Yuichiro Mita, PhD, Osamu Kusano-Arai, Msc, Hiroko Iwanari, PhD, Hiroyoshi Ariga, PhD, Takao Hamakubo, MD, PhD, Yasukazu Yoshida, PhD, Etsuo Niki, PhD, Shigeo Murayama, MD, PhD, Yasuo Ihara, MD, and Noriko Noguchi, PhD

Abstract

DJ-1, the product of a causative gene of a familial form of Parkinson disease, undergoes preferential oxidation of Cys106 (cysteine residue at position 106) under oxidative stress. Using specific monoclonal antibodies against Cys106 oxidized DJ-1 (oxDJ-1), we examined oxDJ-1 immunoreactivity in brain sections from DJ-1 knockout and wild-type mice and in human brain sections from cases classified into different Lewy body stages of Parkinson disease and Parkinson disease with dementia. Oxidized DJ-1 immunoreactivity was prominently observed in neuromelanin-containing neurons and neuron processes of the substantia nigra; Lewy bodies also showed oxDJ-1 immunoreactivity. Oxidized DJ-1 was also detected in astrocytes in the striatum, in neurons and glia in the red nucleus, and in the inferior olivary nucleus, all of which are related to regulation of movement. These observations suggest the relevance of DJ-1 oxidation to homeostasis in multiple brain regions, including neuromelanin-containing neurons of the substantia nigra, and raise the possibility that oxDJ-1 levels might change during the progression of Lewy body–associated neurodegenerative diseases.

From the Systems Life Sciences (YS, KH, YM, NN) and Neuropathology (TM, YI), Department of Medical Life Systems, Faculty of Medical and Life Sciences, Doshisha University, Kyotanabe, Kyoto; Department of Neuropathology, Tokyo Metropolitan Institute of Gerontology (HH, SM); Laboratory of Systems Biology and Medicine, Research Center for Advanced Science and Technology, University of Tokyo (OK-A, HI, TH); and Institute of Immunology Co Ltd (OK-A), Tokyo; Health Research Institute, National Institute of Advanced Industrial Science and Technology, Ikeda, Osaka (YY, EN); and Graduate School of Pharmaceutical Sciences, Hokkaido University, Kita-ku, Sapporo (KT-N, HA), Japan.

Send correspondence and reprint requests to: Yoshiro Saito, PhD, Systems Life Sciences, Department of Medical Life Systems, Faculty of Medical and Life Sciences, Doshisha University, IN333, 1-3 Miyakodani, Tatara, Kyotanabe, Kyoto 610-0394 Japan; E-mail: ysaito@mail.doshisha.ac.jp

This work was supported in part by the Michael J. Fox Foundation, Japan Society for the Promotion of Science Grants-in-Aid for Scientific Research (Grant No. 25670084), Ministry of Education, Culture, Sports, Science, and Technology–Supported Program for the Strategic Research Foundation at Private Universities, and Focus 21 project of the New Energy and Industrial Technology Development Organization.

The authors declare that they have no competing interests.

Supplemental digital content is available for this article. Direct URL citations appear in the printed text and are provided in the HTML and PDF versions of this article on the journal's Web site (www.jneuropath.com).

Key Words: Cysteine, DJ-1, Inferior olivary nucleus, Lewy body, MALDI-TOF MS, Oxidative stress, Parkinson disease, Substantia nigra.

INTRODUCTION

Recent studies, particularly genetic studies, have yielded new insights into molecular mechanisms underlying the pathogenesis of Parkinson disease (PD) (1). The identification of *DJ-1* as a causative gene of a familial form of PD (i.e. *PARK7*) suggests the role of oxidative stress and reactive oxygen species (ROS) in PD pathogenesis (2, 3). DJ-1 is a multifunctional protein involved in several processes, including antioxidative defense and transcriptional regulation (3–6). Nigral dopaminergic neurons are considered to be rich in ROS because both enzymatic and nonenzymatic metabolism of dopamine lead to ROS generation (7). In addition, calcium entry through L-type channels in nigral dopaminergic neurons occurs throughout the pacemaking cycle, leading to the metabolic cost of ATP consumption that results in ROS generation (6). Although the etiology of PD remains unknown, increasing evidence suggests that oxidative stress—defined as an imbalance between oxidants and antioxidants resulting in increased oxidants—is an important mediator of PD pathogenesis (8).

Previous studies have revealed that the cysteine residue at position 106 (Cys106) of DJ-1 is preferentially oxidized in cells exposed to oxidative stress (9). Cysteine forms 3 different oxidized species (i.e. cysteine–sulfenic acid [Cys-SOH], cysteine–sulfinic acid [Cys-SO_2H], and cysteine–sulfonic acid [Cys-SO_3H]) through direct oxygen addition. Two-dimensional (2D) polyacrylamide gel electrophoresis (PAGE) has shown an acidic spot shift of DJ-1 in cells under oxidative stress, and previous studies have shown that these acidic p*I* shifts are caused by a posttranslational process induced by the oxidation of the cysteine residue to Cys-SO_2H or Cys-SO_3H (9). Cysteine–sulfinic acid is chemically unstable and easily oxidized to Cys-SO_3H; however, Cys-SO_2H has been reported to be stable in Cys106 oxidized DJ-1 (oxDJ-1) because of the surrounding amino acid residues (10). The critical role of Cys106 in the biologic function of DJ-1 has also been demonstrated (3, 11). The Cys-SO_2H form of oxDJ-1 is likely the active form, and further oxidation to Cys-SO_3H leads to loss of biologic function (11, 12). Recently, it has been postulated that DJ-1 acts as a sensor of oxidative stress by inducing changes in gene expression levels related to antioxidative defense systems (11).

Our research group has developed specific antibodies against oxDJ-1 (13). Using a competitive enzyme-linked immunosorbent assay to detect oxDJ-1, we found that oxDJ-1 levels in the erythrocytes of unmedicated PD patients were markedly higher than oxDJ-1 levels in the erythrocytes of medicated PD patients (treated with L-3,4-dihydroxyphenylalanine and/or dopamine agonist) or healthy subjects (13). We also reported that animal models of PD, prepared by administration of neurotoxins such as 6-hydroxydopamine and 1-methyl-4-phenyl-1,2,3,6-tetrahydropyridine, are involved in the oxidative modification of DJ-1 in the brain and in erythrocytes (14). Based on immunohistochemical analyses of 1-methyl-4-phenyl-1,2,3,6-tetrahydropyridine–treated mice, the number of oxDJ-1–positive cells exhibiting astrocyte-like morphology increased in a dose-dependent manner.

Previous immunohistochemical studies revealed that DJ-1 is abundantly expressed in the reactive astrocytes of patients with neurodegenerative diseases (15, 16). Several studies have also reported that DJ-1 is not an essential component of Lewy bodies (LBs)—the pathologic hallmark of PD (15, 16); however, DJ-1 is present in a subpopulation of glial and neuronal tau inclusions in tau pathology (16–18). Furthermore, generation of the acidic p*I* isoform of DJ-1 in the brains of patients with PD has been reported (15, 19); however, detailed distribution of oxDJ-1 in the human brain has yet to be elucidated.

Here, we used immunohistochemical analyses with specific antibodies against oxDJ-1 to determine the levels and distributions of oxDJ-1 in the brains of a mouse model and of PD patients. The diseases studied included PD and control subjects with different LB stages and PD with dementia (PDD). We also assessed the molecular composition of oxDJ-1 and DJ-1 in frozen brain samples of patients with neurodegenerative diseases of different LB stages.

MATERIALS AND METHODS

Chemicals

Hydrogen peroxide (H_2O_2) and isopropyl-β-D-1-thiogalactopyranoside were purchased from Wako Pure Chemical Industries (Osaka, Japan); anti–β-actin (AC-15) was purchased from Sigma-Aldrich (St Louis, MO); nickel–nitrilotriacetic acid agarose was purchased from QIAGEN (Hilden, Germany); and a protease inhibitor cocktail tablet was purchased from Nacalai Tesque (Kyoto, Japan). Dulbecco modified Eagle medium/nutrient mixture F-12 ham (1:1) was purchased from Invitrogen (Carlsbad, CA), and fetal bovine serum (GPK0029) was purchased from Hyclone (Logan, UT). The polyclonal antibody against phosphorylated α-synuclein was kindly provided by Dr Iwatsubo (University of Tokyo, Tokyo, Japan). SH-SY5Y cells were obtained from the American Tissue Type Collection (Manassas, VA). Other chemicals used were of the highest quality commercially available.

Preparation of Cys106 OxDJ-1 Recombinant Protein

Full-length human DJ-1 complementary DNA (570 bp; NM_007262) was cloned into pEXP1-DEST and transformed into *Escherichia coli* strain BL21(DE3)pLysS; a fusion protein was obtained with a 6-His tag at the amino terminus. The bacterial culture was grown in Luria-Bertani medium with 50 μg/mL ampicillin until the absorbance value of the medium at 600 nm had reached 0.5. Protein expression was induced by the addition of 0.5 mmol/L isopropyl-β-D-1-thiogalactopyranoside. After 2 hours, DJ-1 in the cells was oxidized by treatment with 50 mmol/L H_2O_2 for 15 minutes at 37°C. The cells were then treated with lysozyme and disrupted by sonication in native purification buffer (50 mmol/L $NaHPO_4$ and 0.5 mol/L NaCl, pH 8.0). The supernatant was incubated with nickel–nitrilotriacetic acid agarose, and the 6-His tag fusion protein was eluted with native purification buffer containing 250 mmol/L imidazole. For further analysis, the impurities of imidazole and NaCl were removed by passing the eluent through a PD-10 gel filtration column equilibrated with the desired buffer.

The oxidation of Cys106 was confirmed by matrix-assisted laser desorption/ionization (MALDI) time-of-flight (TOF) mass spectrometry (MS). Purified recombinant proteins (5 μg of protein) were separated by 12.5% sodium dodecyl sulfate (SDS)–PAGE under reducing conditions (1% mercaptoethanol) and by staining with Coomassie Brilliant Blue R-250. The stained band was excised, treated with 25 mmol/L ammonium bicarbonate (pH 8.8) containing 50% acetonitrile, and dehydrated with acetonitrile. The gel pieces were then rehydrated in 25 mmol/L ammonium bicarbonate solution containing 10 mmol/L dithiothreitol and alkylated with 55 mmol/L iodoacetamide. After dehydration with acetonitrile, the gel pieces were rehydrated on ice for 30 minutes in 50 mmol/L ammonium bicarbonate solution containing 10 μg/mL sequence-grade modified trypsin (Promega, Madison, WI). In-gel digestion was performed for 18 hours at 37°C. The resulting peptides were extracted with 5% trifluoroacetic acid in 50% acetonitrile. The extracts were concentrated to 10 μL using a SpeedVac (Thermo Electron, Waltham, MA). The samples were mixed with α-cyano-4-hydroxycinnamic acid and subjected to MALDI-TOF MS analysis (4800 Plus; AB SCIEX, Framingham, MA). For detailed sequence analysis, peptide samples were separated and spotted on a plate for MALDI-TOF MS using a capillary liquid chromatography system coupled to an autospotter (DiNa ASM-T-MaP; KYA TECH, Tokyo, Japan). Data were processed using the ProteinPilot 3.0 software (AB SCIEX). UniProtKB/Swiss-Prot protein databases were used to identify peptide fragments.

Preparation of Antibodies Against OxDJ-1

Monoclonal antibodies (mAbs) against oxDJ-1 were prepared as follows. Briefly, the oxDJ-1 recombinant protein (40 μg) was mixed in Freund complete adjuvant and injected into mice. All animal experiments described in this study fully conformed to the guidelines outlined in the Guide for the Care and Use of Laboratory Animals of Japan and were approved by the Animal Care Committee of Doshisha University (approval number 1053). The animals were killed 6 weeks after the initial immunization. Cells from the spleen were used for cell fusion, hybridization, cloning, and establishment of hybridomas. Screening for the production of anti–oxDJ-1 antibodies was conducted by ELISA and Western blot analysis.

SDS-PAGE and 2D-PAGE for Western Blot Analysis and Silver Staining

Preparation of whole-cell extracts, SDS-PAGE, and 2D-PAGE were conducted as previously described (20, 21). To obtain whole-cell extracts of human neuroblastoma SH-SY5Y cells and DJ-1 knockout (KO) fibroblasts (22) for PAGE, we collected the cells, washed them with ice-cold phosphate-buffered saline (PBS), and resuspended them in lysis buffer (150 mmol/L NaCl, 50 mmol/L Tris-HCl [pH 7.4], 50 mmol/L NaF, 5 mmol/L ethylenediaminetetraacetic acid, 0.5% Triton X-100, 1 mmol/L Na_3VO_4, and a protease inhibitor cocktail tablet) at 4°C for 30 minutes. Cellular debris was removed by centrifugation at 15,000 × *g* for 5 minutes. Protein concentration was determined using the bicinchoninic acid protein assay kit (Pierce Biotechnology, Rockford, IL) with bovine serum albumin as standard.

For Western blot analysis, cell lysates (15 μg of protein) from each sample were reduced and denatured in 63 mmol/L Tris-HCl (pH 6.8) containing 1% mercaptoethanol, 2% SDS, 5% sucrose, and 0.012% bromophenol blue for 5 minutes at 95°C. The reduced protein mixture was then separated on a 12.5% SDS-PAGE gel. For the first dimension of 2D-PAGE, immobilized pH gradient gel strips (pH 4–7; nonlinear, 7 and 13 cm; GE Healthcare Bioscience, Uppsala, SE) were used. The samples (15 μg of protein) were mixed with sample buffer (9 mol/L urea, 5% 3-[(3-cholamidopropyl)dimethylammonio] propanesulfonate, 65 mmol/L dithioerythritol, and 0.5% ampholyte [pH 4–7]), applied on a gel, and rehydrated for 18 hours. Electrophoresis voltage was increased stepwise to 5,000 or 8,000 V at a maximal current of 200 mA for 3 to 5 hours. Each strip was equilibrated in 50 mmol/L Tris-HCl (pH 8.8) containing 6 mol/L urea, 2% SDS, 30% glycerol, and 20 mmol/L dithioerythritol for 20 minutes. Second-dimension separation was achieved by performing SDS-PAGE in the manner described previously.

After separation by either SDS-PAGE or 2D-PAGE, the samples were transferred to an Immobilon-P Transfer Membrane (Millipore, Billerica, MA) for Western blot analysis. The membranes were blocked with 5% skim milk powder (Snow Brand Milk Products, Tokyo, Japan); dissolved in Tris-buffered saline (TBS; pH 7.4) containing 0.1% Tween 20; incubated with mouse anti–oxDJ-1 mAbs (clones M106 and M149), mouse anti–DJ-1 mAb (clone 3E8; Medical and Biological Laboratories, Nagoya, Japan), or rabbit anti–DJ-1 mAb (clone EP2816Y; GeneTex, Irvine, CA) at 4°C for 18 hours; washed with TBS (pH 7.4) containing 0.1% Tween 20; incubated with horseradish peroxidase–conjugated secondary antibodies for at least 1 hour; and washed with TBS (pH 7.4) containing 0.1% Tween 20. Immunoreactivity (IR) of these antibodies was visualized using Immobilon Western (Millipore) and LAS-4000 (Fujifilm, Tokyo, Japan). Relative densities were determined using the Multi Gauge software (Fujifilm). For silver staining, the separated proteins were stained using the Dodeca Silver Stain Kit (Bio-Rad Laboratories, Hercules, CA).

Preparation of Brain Sections From Mice

Paraffin-embedded sections of wild-type and DJ-1 KO mice (B6.Cg-Park7^{tm1Shn}/L; The Jackson Laboratory, Bar Harbor, ME) were prepared as previously described (14). Whole brains of wild-type and DJ-1 KO mice were removed immediately after anesthetization with pentobarbital, and subsequent transcardial perfusion was performed with PBS and 4% paraformaldehyde in PBS. The samples were then fixed overnight with paraformaldehyde in PBS at 4°C and embedded in paraffin.

Immunohistochemistry

Paraffin-embedded sections (5 μm) from each brain tissue were stained using immunohistochemistry with anti–oxDJ-1 mAbs (clones M106 and M149) or anti–DJ-1 mAbs (clones 3E8 and EP2816Y). After deparaffinization, the sections were incubated with 10% normal goat serum in 50 mmol/L Tris-HCl (pH 7.4) containing 150 mmol/L NaCl (TBS) at room temperature, and the sections were incubated overnight with primary antibodies such as the oxDJ-1 mAb (2 μg/mL). The sections were incubated for 2 hours with the biotinylated secondary antibody then incubated for 30 minutes at room temperature with the avidin-biotin-peroxidase complex (Vector Laboratories, Burlingame, CA). To examine antibody binding, we incubated the sections with 3,3-diaminobenzidine in the presence of H_2O_2. The sections were then lightly counterstained with hematoxylin. To evaluate staining specificity, we stained some sections in the absence of primary antibodies. In addition, we also examined absorption with the oxDJ-1 recombinant protein; however, oxDJ-1 IR inversely increased (data not shown). This observation suggests the binding of the oxDJ-1 recombinant protein to the brain tissues under the conditions used. All stained sections were photographed under a light microscope connected to a charge-coupled device camera.

For confocal microscopy, lipofuscin autofluorescence was eliminated with Sudan Black B then sections were incubated with primary antibodies. Bound antibodies were visualized with Alexa 488–conjugated anti-mouse IgG or Alexa 568–conjugated anti-rabbit IgG (Molecular Probes, Eugene, OR). Specimens were observed using a laser-scanning microscope (LSM 710 ConfoCor 3; Carl Zeiss, Thornwood, NY) equipped with Zeiss Efficient Navigation 2009 software.

Human Brain Tissues

The postmortem brains of 21 patients were studied. Frozen brain tissues and paraffin-embedded sections from controls and patients with PD and PDD were obtained from the Brain Bank for Aging Research at the Tokyo Metropolitan Institute of Gerontology. Lewy body pathology was classified into 6 LB stages according to our previously published criteria (23): LB stage 0, no LBs; LB stage I, scattered LBs without cell loss; LB stage II, abundant LBs with macroscopic loss of pigmentation in the substantia nigra (SN) and locus ceruleus and/or gliosis demonstrated by immunohistochemistry for glial fibrillary acidic protein in areas containing LBs but without attributable parkinsonism or dementia; LB stage III, PD without dementia; LB stage IV, dementia with LBs, transitional (limbic) form; LB stage V, dementia with LBs, neocortical form (diffuse LB disease). Because of the controversy surrounding the definition of PDD, we included PDD as a subgroup in LB stages IV and V. PD, PDD, and dementia with

TABLE 1. Clinical and Postmortem Details and OxDJ-1 Staining of Cases Included in the Present Study

Patient No.	Sex	Age, y	Postmortem Interval, hours:minutes	Cause of Death	Newcastle Staging	Braak Staging	OxDJ-1 staining*		
							SN	ST	ION
LS 0 (controls)									
1	F	104	6:55	Heart failure	NA	0	+	+	+
2†	F	79	1:35	Myocardial infarction	NA	0	+++	+++	+++
3	F	80	18:31	GI tract hemorrhage	NA	0	+	++	++
4	M	71	13:54	Pneumonia	NA	0	+	+	+
LS I									
5	M	92	4:10	Pneumonia	NA	2	++	+++	++
6†	F	82	17:30	Aortic dissection	NA	2	++	+++	+
7†	F	93	2:09	Pneumonia	NA	2	+++	+	+++
8†	F	79	17:08	Suffocation caused by aspiration	NA	1	++	+	+++
LS II									
9	F	93	7:42	Heart failure	NA	3	++	++	+
10	F	90	2:52	Heart failure	NA	3	+++	+++	+
11	F	80	5:56	Respiratory failure	NA	3	+++	+++	++
12†	M	84	14:00	Heart failure	NA	3	+++	+++	+++
LS III–PD									
13†	M	81	2:01	Tongue cancer	BSP	4	++	++	+
14†	M	88	18:45	Pneumonia	BSP	4	+++	+++	++
15	M	81	12:32	Tuberculosis	BSP	4	+++	++	++
LS IV–PDD									
16†	M	72	18:12	Pneumonia	Lmb-trans	5	++	++	++
17	M	72	6:05	Sepsis	Lmb-trans	5	+	−	++
18†	F	79	2:30	Neurogenic shock	Lmb-trans	5	++	+	−
19†	M	85	14:42	Pneumonia	Lmb-trans	5	−	++	−
20†	F	79	4:52	Respiratory failure	Lmb-trans	4	+	−	+
LS V–PDD									
21†	M	83	10:18	Pneumonia	Diffuse neocortical	6	−	−	−

Lewy body (Newcastle) staging and Braak staging were based on McKeith et al (26).
Newcastle staining refers to LB type (26).
* Qualitative rating scales used for oxDJ-1 immunohistochemical staining of each site. Brain sections were evaluated by visual observation and classified as (−) none, (+) mild, (++) moderate, or (+++) severe.
† Case samples used for biochemical analysis.
BSP, brainstem predominant; F, female; GI, gastrointestinal; Lmb-trans, limbic (transitional); M, male; NA, not assigned; ST, striatum.

LBs were diagnosed based on previously reported criteria (24–26). Detailed clinical and pathologic data are presented in Table 1. This study was approved by the local ethics committees of the Tokyo Metropolitan Institute of Gerontology and Doshisha University (approval number 0920).

Tissue Fractionation

Brain tissues were homogenized with a motor-driven Teflon homogenizer in TBS (50 mmol/L Tris-HCl [pH 7.6] and 0.15 mol/L NaCl) containing a protease inhibitor cocktail, as described previously (27). The homogenates were spun for 10 minutes at 3,000 × *g*, and the supernatants from the homogenates were then centrifuged at 540,000 × *g* for 20 minutes. The resulting TBS-insoluble pellets were resuspended in TBS containing 1% sodium dodecyl sarcosinate (sarkosyl). After incubation for 30 minutes at 4°C, the suspensions were centrifuged at 540,000 × *g* for 20 minutes. The pellets obtained (containing the sarkosyl-insoluble fraction) were resuspended in TBS containing 1% SDS then ultracentrifuged. Finally, the 1% SDS-insoluble pellets were suspended by vigorous sonication in SDS sample buffer. After the protein concentration had been determined with the bicinchoninic acid method, each fraction was subjected to Western blot analysis as described previously.

Statistical Analysis

The statistical significance of the difference between determinations was calculated by Student t-test. Values of $p < 0.05$ were considered significant.

RESULTS

Characterization of OxDJ-1–Specific mAbs

Specific antibodies against oxDJ-1 (clones M106 and M149) were prepared using the oxDJ-1 recombinant protein as antigen (13). Specificity was evaluated by Western blot analyses of proteins separated by SDS-PAGE and 2D-PAGE and compared with anti–DJ-1 antibodies (commercially available clones 3E8 and EP2816Y) (15). Oxidation of Cys106 to Cys-SO_3H in the oxDJ-1 recombinant protein was confirmed by MALDI-TOF MS analysis. These data and the tandem MS (MS/MS) spectrum

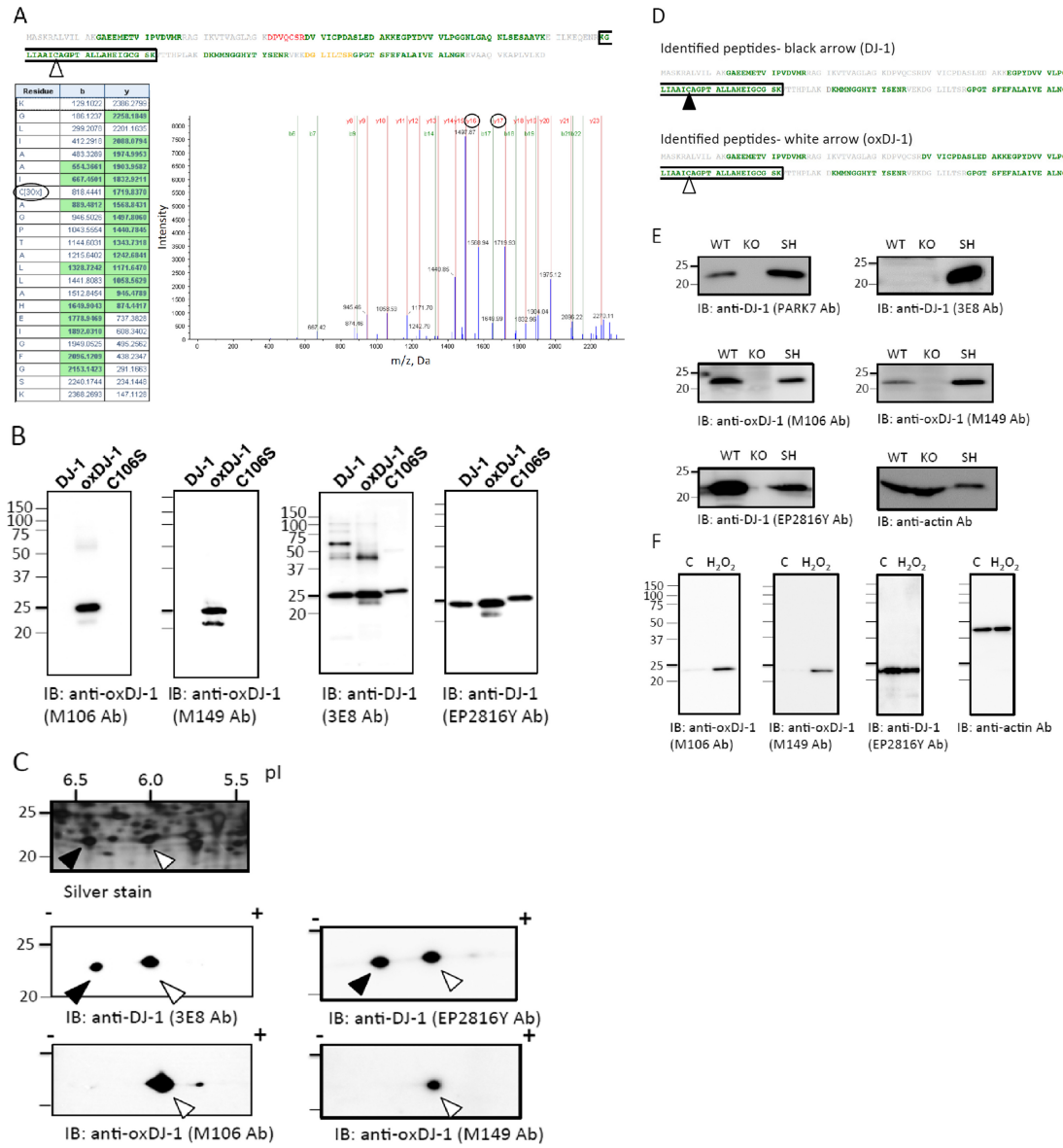

FIGURE 1. Characterization of antibodies against oxDJ-1. **(A)** Matrix-assisted laser desorption/ionization TOF MS analysis of recombinant oxDJ-1. Recombinant oxDJ-1 (5 μg) was separated by SDS-PAGE, and the Coomassie Brilliant Blue R-250–stained band was subjected to in-gel digestion. Peptide samples were analyzed by MALDI-TOF MS. Identified peptide sequences with confidence intervals greater than 95% are shown in green. The sequences indicated by yellow and red correspond to confidence intervals higher than 50% and lower than 50%, respectively. The MS/MS spectrum of peptides predicted to contain Cys106-SO_3H. The MS/MS spectrum provides sequence data for unequivocal assignment of oxDJ-1 (100–122), the Cys that is oxidized to Cys-SO_3H (white arrowhead). **(B)** Selectivity of anti–oxDJ-1 mAbs against the oxDJ-1 recombinant protein. Fifty nanograms of DJ-1, oxDJ-1, and C106S-DJ-1 was separated by SDS-PAGE and subjected to Western blot analysis using anti–oxDJ-1 (clones M106 and M149) and anti–DJ-1 (clones 3E8 and EP2816Y) antibodies. **(C)** Specific reactivity of anti–oxDJ-1 antibodies against oxDJ-1 in SH-SY5Y cells. Cell lysates (200 μg for silver staining and 15 μg for Western blot analysis) obtained from SH-SY5Y cells were separated by 2D-PAGE and subjected to silver staining and Western blot analyses using anti–DJ-1 and anti–oxDJ-1 antibodies. Black and white arrowheads indicate native DJ-1 (calculated p*I* = 6.4) and oxDJ-1 (calculated p*I* = 6.0), respectively. **(D)** Matrix-assisted laser desorption/ionization TOF MS analysis of the DJ-1 spot in SH-SY5Y cell lysates. The stained spots corresponding to DJ-1 (black arrowhead) and oxDJ-1 (white arrowhead) were subjected to in-gel digestion and analyzed by MALDI-TOF MS. Peptides containing Cys106-SH and Cys106-SO_3H are shown in black and white black arrowheads, respectively. **(E)** Evaluation of the specificity of the DJ-1 and oxDJ-1 antibodies using total lysates from DJ-1 KO fibroblasts. Cell lysates (15 μg) obtained from wild-type (WT) and DJ-1 KO fibroblasts and SH-SY5Y cells (SH) were separated by SDS-PAGE and subjected to Western blot analyses using anti–DJ-1 and anti–oxDJ-1 antibodies. **(F)** Detection of oxDJ-1 with anti–oxDJ-1 antibodies in H_2O_2-treated SH-SY5Y cells. Cell lysates (15 μg) obtained from cells treated with 0 or 1 mmol/L H_2O_2 for 30 minutes were separated by SDS-PAGE and subjected to Western blot analysis using the DJ-1 and oxDJ-1 antibodies. IB, immunoblot.

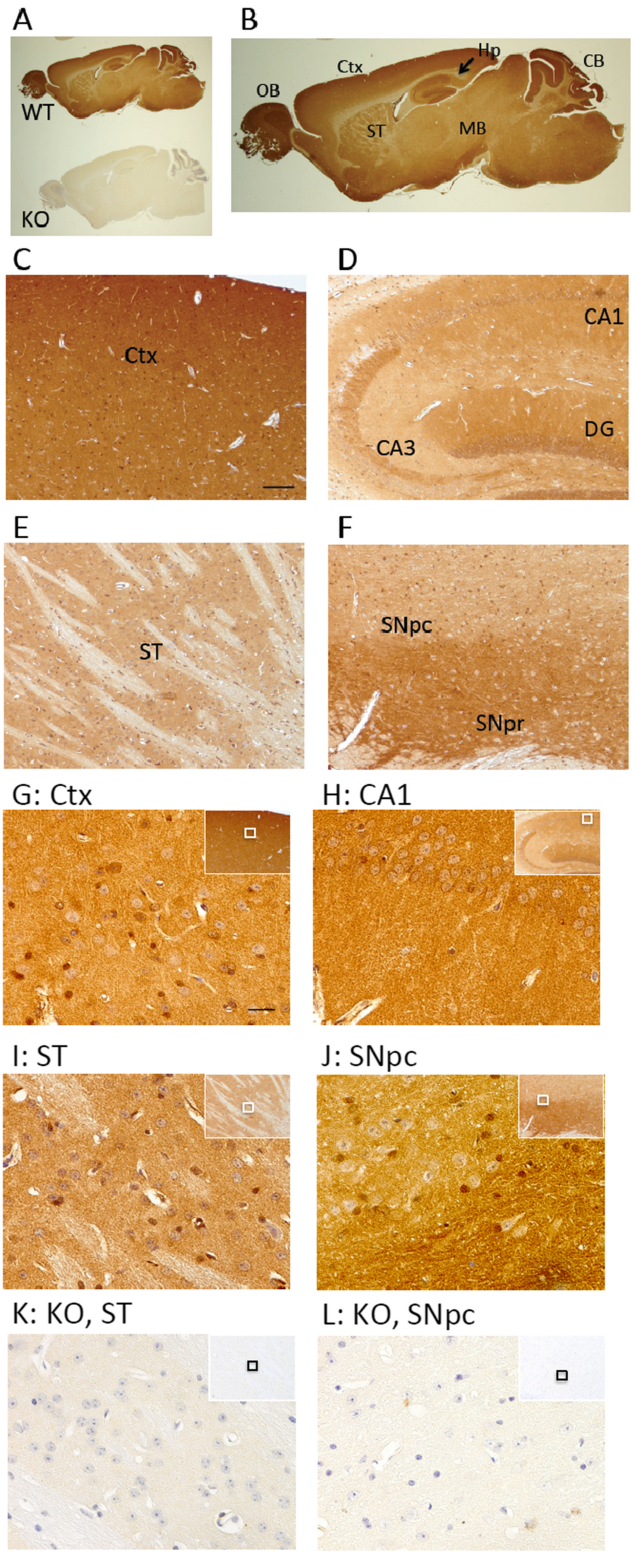

FIGURE 2. Immunohistochemical distribution of the oxDJ-1 protein in the mouse brain. **(A, B)** Sagittal sections from wild-type (WT) and DJ-1 KO mice brains were stained with anti–oxDJ-1 mAbs. Immunoreactivity of the anti–oxDJ-1 mAb (clone M149) was present throughout the brain and was absent in the DJ-1 KO mouse brain. **(C–J)** High magnification of the cerebral cortex (Ctx) **(C, G)**, hippocampus (Hp) **(D, H)**, striatum (ST) **(E, I)**, SN pars compacta (SNpc), and SN pars reticulata (SNpr) **(F, J)** of WT mice. **(K, L)** High magnification of the ST **(K)** and SNpc **(L)** of DJ-1 KO mice. Scale bars = **(C)** 100 μm (applies to **C–F**); **(G)** 20 μm (applies to **G–L**). Similar IR patterns were observed using the anti–oxDJ-1 mAb (clone M106). CB, cerebellum; DG, dentate gyrus; MB, midbrain; OB, olfactory bulb.

TABLE 2. Distribution of OxDJ-1 in Human and Mouse Brains

Area	Obvious Staining Site	Cell Types	Others	Note
Mouse				
Midbrain	SN	Neuronal cells (cell bodies), glial cells (nucleus)	Neuropil	—
Striatum	—	Small to medium spiny neurons (cell bodies), glial cells (nucleus)	Neuropil	—
Hippocampus	CA1	Pyramidal cells (cell bodies)	Stratum radiatum, mossy fibers, neuropil	—
	DG	Granule cells	Moleculare layer	—
Cortex	Laminae	Neuronal cells (cell bodies), glial cells (nucleus)	Neuropil	—
Cerebellum	—	—	—	—
Olfactory bulb	—	—		
Human				
Midbrain	SN	Dopaminergic neuronal cells (cell bodies, neurites)	Neuropil, colocalization with LB	Increase in LS II and III–PD, decrease in LS IV– and LS V–PDD
	RN	Glial cells (cell bodies, nucleus, neurites)	Neuropil	—
Striatum	Putamen	Astrocytes (cell bodies, nucleus, neurites)	Neuropil	Increase in LS II and LS III–PD, decrease in LS IV– and LS V–PDD
Medulla oblongata	VNDN	Neuronal cells (cell bodies, neurites)	Neuropil, colocalization with LB	—
	ION	Neuronal cells (cell bodies, nucleus, neurites), glial cells (cell bodies, nucleus, neurites)	Neuropil	—

(—) No immunostaining present; CA1, cornu ammonis 1; DG, dentate gyrus; RN, red nucleus.

of Cys106 oxidation are shown in Figure 1A. The 2 antibodies against oxDJ-1 revealed strong reactivity against the oxDJ-1 recombinant protein, with less reactivity against DJ-1 or C106S-DJ-1, in which Cys106 had been substituted for Ser (Fig. 1B). In contrast, antibody clones 3E8 and EP2816Y, which bound both DJ-1 and oxDJ-1, detected all recombinant proteins (Fig. 1B). Human neuroblastoma SH-SY5Y cell lysates were separated by 2D-PAGE and subjected to Western blot analysis using antibodies against oxDJ-1 (M106 and M149) and DJ-1 (3E8 and EP2816Y). A peptide containing Cys106-SO_3H was detected in the acidic spot of DJ-1 shown by silver staining (Fig. 1C, white arrowhead); Cys106-SO_3H was not detected in the native DJ-1 spot (Fig. 1C, black arrowhead). Mass spectrometry data are summarized in Figure 1D. Consistent with this observation, a spot corresponding to oxDJ-1 was observed in 2D Western blot analysis using anti–oxDJ-1 antibodies (Fig. 1C, white arrowheads).

The specificity of the mAbs used in the present study was further confirmed using a whole-cell lysate of fibroblasts from DJ-1 KO mouse. Reactivity of the human DJ-1–specific mAb 3E8 to mouse DJ-1 was not observed; however, specific reactivity was confirmed for other antibodies used in the present study (Fig. 1E). Finally, the specificity of anti–oxDJ-1 mAbs was further confirmed using H_2O_2-treated SH-SY5Y cells. Western blot analysis using both anti–oxDJ-1 mAbs M106 and M149 revealed that the band intensity of oxDJ-1 increased in H_2O_2-treated SH-SY5Y cells, whereas a significant change in band intensity was not observed on Western blot analysis using the anti–DJ-1 mAb EP2816Y (or an anti-actin antibody) (Fig. 1F). Collectively, these data strongly suggest that the anti–oxDJ-1 mAbs used in the present study specifically react with oxDJ-1.

Immunohistochemical Localization of OxDJ-1 in the Mouse Brain

To examine the levels and distribution of oxDJ-1 in the brain, we performed immunohistochemical studies using mAbs against oxDJ-1 in brain sections derived from wild-type and DJ-1 KO mice. The specificity of oxDJ-1 staining by clone M149 was confirmed by the absence of IR in the DJ-1 KO mouse brain (Fig. 2A). The mAb clone M106 also exhibited specific staining and displayed a similar pattern of reactivity as mAb clone M149 (data not shown). On the other hand, DJ-1 staining was also conducted using the antibody EP2816Y, for which specificity could be confirmed by the absence of IR in the DJ-1 KO mouse brain (Figure, Supplemental Digital Content 1, part A, http://links.lww.com/NEN/A603). At low magnification, immunohis tochemical staining revealed that both DJ-1 and oxDJ-1 were expressed throughout the brain (Fig. 2B; Figure, Supplemental Digital Content 1, part B, http://links.lww.com/NEN/A603). Oxidized DJ-1 IR was particularly prominent in the olfactory bulb, cerebellum, cortex, and hippocampus (Fig. 2B). DJ-1 IR was also observed in these areas (Figure, Supplemental Digital Content 1, part B, http://links.lww.com/NEN/A603). In the cerebral cortex, oxDJ-1 IR was evident throughout the laminae, with minimal staining in the corpus

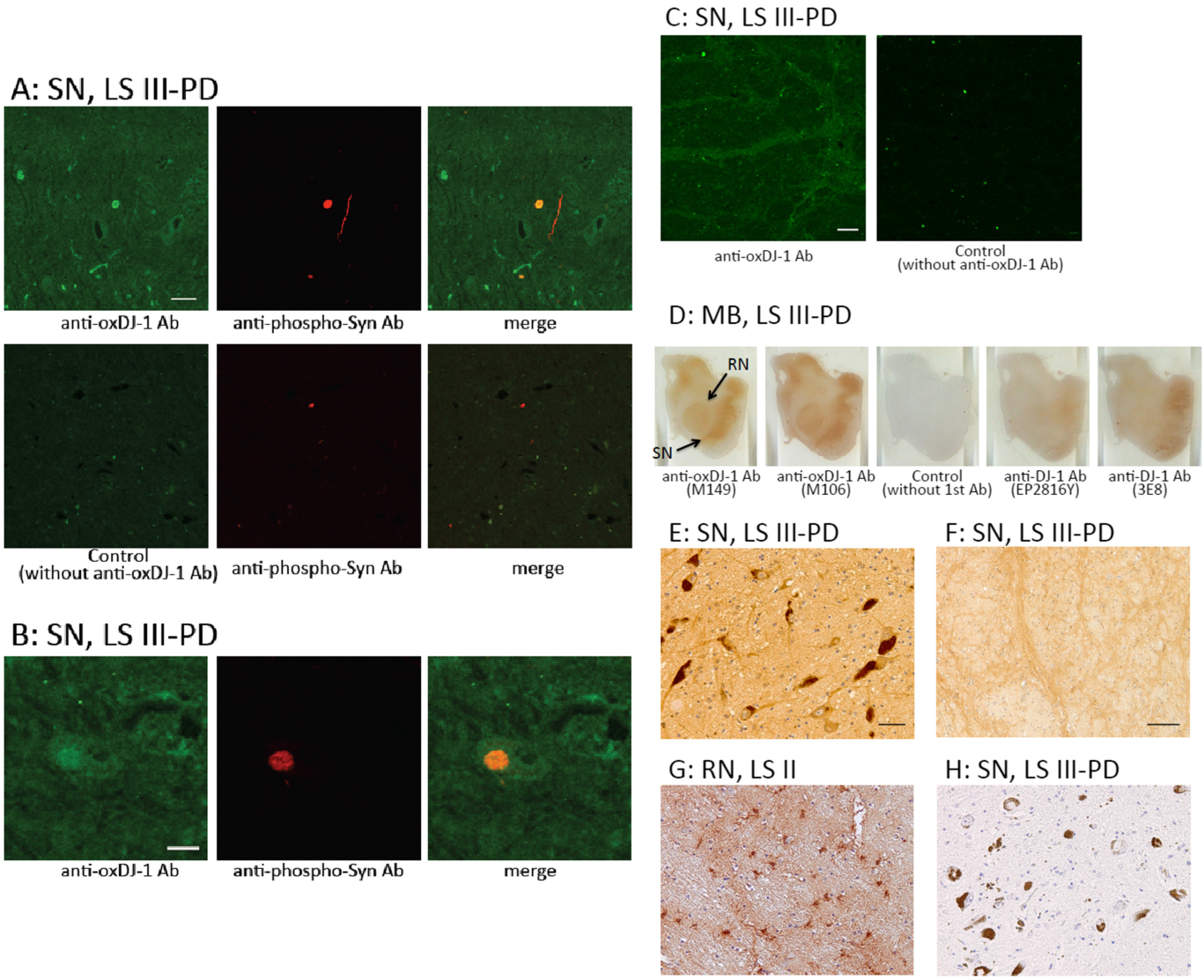

FIGURE 3. Immunohistochemical distribution of oxDJ-1 in the human midbrain. **(A–C)** Confocal images of oxDJ-1 in dopaminergic nigral neuronal cells. A section containing the SN was immunostained with a mAb against oxDJ-1 and a polyclonal antibody against phosphorylated α-synuclein and then visualized using fluorescence confocal microscopy. **(A)** Staining with only the secondary antibody is shown in the lower panel. **(B)** Immunoreactivity of the anti–oxDJ-1 mAb was widely distributed throughout the cell bodies and neurites in dopaminergic neurons of the SN. The areas labeled with anti–oxDJ-1 and anti-phosphorylated α-synuclein (indicative of LBs) antibodies were colocalized **(A)**. Higher magnification is shown in **(B)**. At the periphery of the SN, oxDJ-1 IR was clearly observed in neuron processes **(C)**. **(D)** Oxidized DJ-1 IR was present throughout the midbrain; particularly high levels were observed in the SN and red nucleus (RN). No staining with only the secondary antibody and less staining with the anti–DJ-1 mAbs (clones EP2816Y and 3E8) are shown. **(E–H)** Staining results at higher magnification of the SN **(E, F, H)** and RN **(G)** using the oxDJ-1 mAb **(E–G)** and only the secondary antibody **(H)**. There was IR of cell bodies and processes of neuromelanin-containing neurons with the oxDJ-1 mAb **(E)**; there was no staining with the secondary antibody alone **(H)**. At the periphery of the SN, oxDJ-1 IR was evident in neuron processes **(F)**. In the RN, there was oxDJ-1 IR of glial cells and neuron processes **(G)**. Scale bars = **(A, C, E)** 50 μm; **(B, F)** 20 μm. LB I, patient with scattered LBs without cell loss; LS II, patient with LBs and cell loss but without clinical parkinsonism or dementia; LS III–PD, patients with LB and PD; MB, midbrain.

callosum (Figs. 2B, C). DJ-1 staining in the cerebral cortex is shown in Figure, Supplemental Digital Content 1, parts B and C, http://links.lww.com/NEN/A603. In the hippocampus, pyramidal cells showed oxDJ-1 IR throughout the perikaryon in cornu ammonis subfields (Fig. 2D). In cornu ammonis 1, oxDJ-1 IR of the stratum radiatum was evident, and oxDJ-1 immunostaining of mossy fibers was also observed. In the dentate gyrus of the hippocampus, oxDJ-1 IR in granule cells and moleculare layer was also evident (Fig. 2D). DJ-1 immunostaining in the hippocampus is shown in Figure, Supplemental Digital Content 1, part D, http://links.lww.com/NEN/A603. Oxidized DJ-1 IR was observed in the striatum (Fig. 2E). In the SN, oxDJ-1 IR

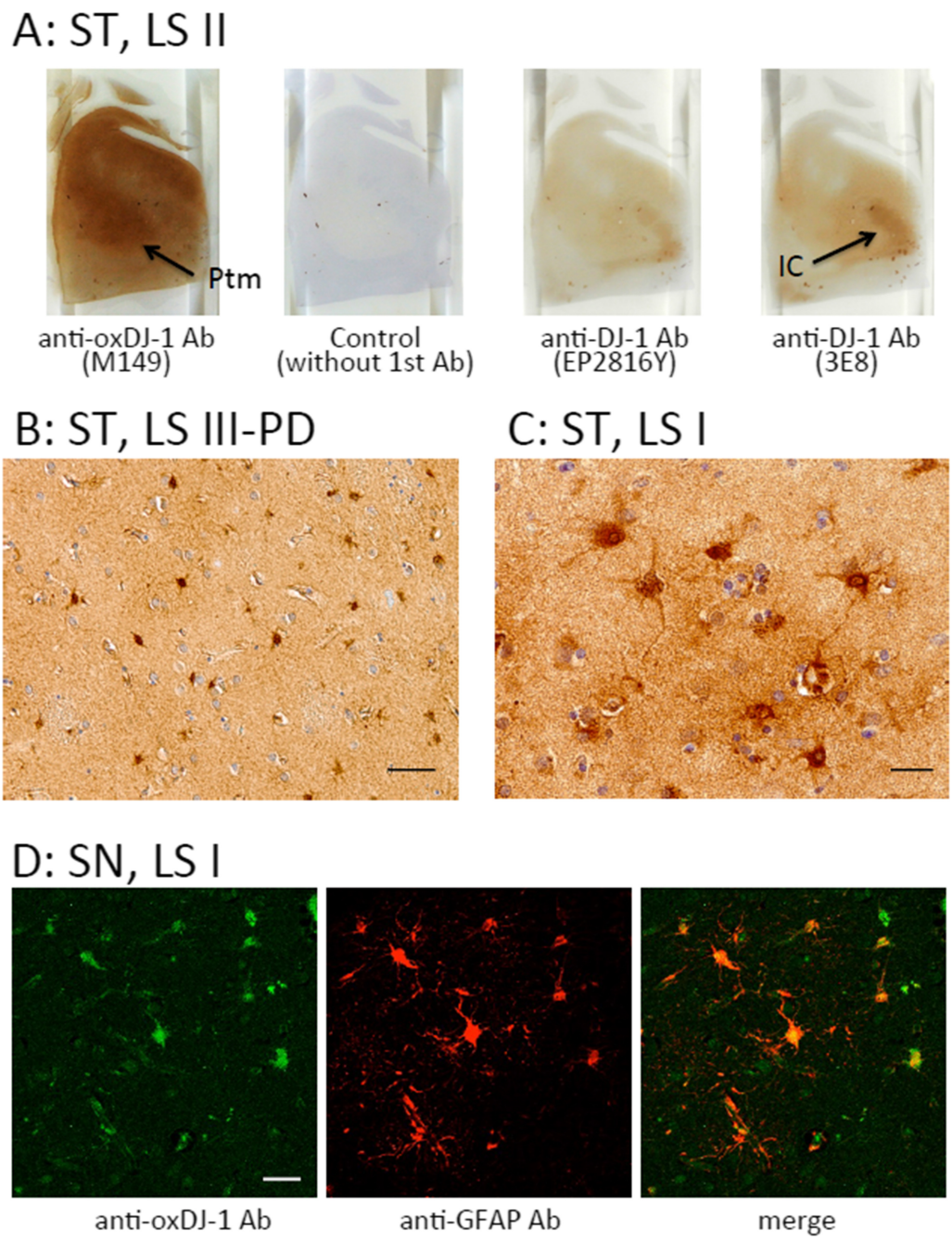

FIGURE 4. Immunohistochemical distribution of the oxDJ-1 protein in the human striatum (ST). **(A)** Immunoreactivity of the anti–oxDJ-1 mAb was present throughout the striatum; particularly high IR was observed in the putamen (Ptm; arrow). There was no staining with the secondary antibody alone. With the anti–DJ-1 mAbs (clones EP2816Y and 3E8), there was staining of the internal capsule (IC; arrow). **(B, C)** Immunostaining of the ST with the anti–oxDJ-1 mAb at high magnification; there was IR of cell bodies and proximal processes of glial cells. **(D)** Confocal microscopy images of oxDJ-1 in ST astrocytes. A section of the ST was immunostained for both oxDJ-1 and glial fibrillary acidic protein and visualized using fluorescence confocal microscopy. Portions labeled with the oxDJ-1 and glial fibrillary acidic protein (astrocytes) antibodies were colocalized. Scale bars = **(B, D)** 50 μm; **(C)** 20 μm. LS II, patient with LBs but without clinical parkinsonism or dementia; LS III–PD, patients with LB and PD.

was evident (Fig. 2F). DJ-1 IR in the SN was also observed as shown in Figure, Supplemental Digital Content 1, part F, http://links.lww.com/NEN/A603.

At high magnification, oxDJ-1 IR was enriched in the perikaryon of neuronal cells, in the nuclei of glial cells, and in neuropil in the cerebral cortex (Fig. 2G). In the hippocampus, cell bodies of cornu ammonis 1 pyramidal cells and neuropil showed oxDJ-1 IR (Fig. 2H). In the striatum, oxDJ-1 IR was present within the cell bodies of small to medium spiny neurons, glial cell nuclei, and neuropil (Fig. 2I). In the SN pars compacta,

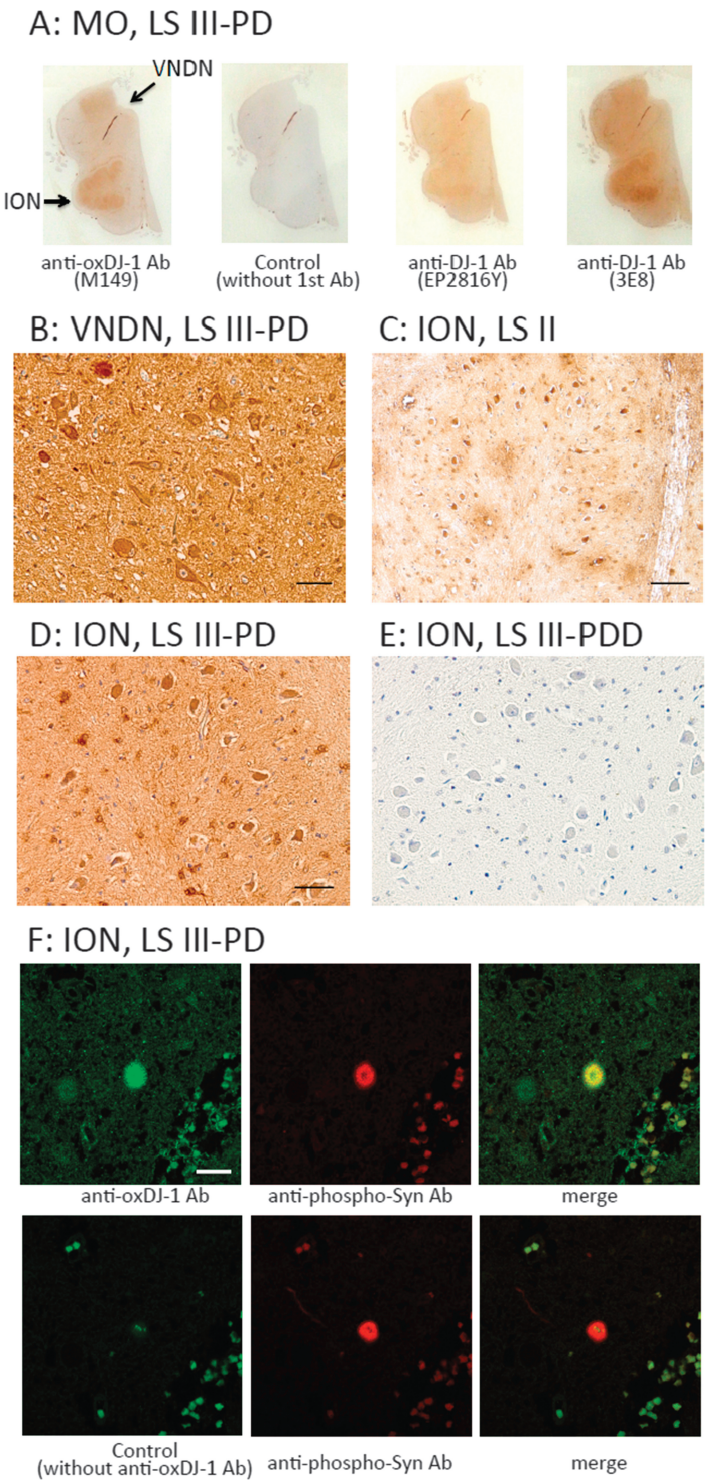

FIGURE 5. Immunohistochemical distribution of the oxDJ-1 protein in the human medulla oblongata. **(A)** Immunoreactivity of the anti–oxDJ-1 mAb in the medulla oblongata; there was particularly high oxDJ-1 IR in the ION (arrow). There was no IR with the secondary antibody alone; there was less IR with the anti–DJ-1 mAbs (clones EP2816Y and 3E8). **(B–E)** Staining results of the medulla oblongata with the oxDJ-1 mAb **(B–D)** and the secondary antibody only **(E)** at higher magnification. In the VNDN and ION, there was IR in neuronal and glial cells. **(F)** Confocal images of oxDJ-1 in the VNDN. A brain section containing the VNDN was simultaneously immunostained for both oxDJ-1 and phosphorylated α-synuclein and then visualized using fluorescence confocal microscopy. Staining with only the secondary antibody is shown in the lower panel of **(F)**. The portions labeled with anti–oxDJ-1 mAb and anti-phosphorylated α-synuclein (indicative of LBs) antibody colocalized. Scale bars = **(B, D)** 50 μm; **(C)** 100 μm; **(F)** 20 μm. LS II, patient with LBs but without clinical parkinsonism or dementia; LS III–PD, patients with LB and PD; MO, medulla oblongata.

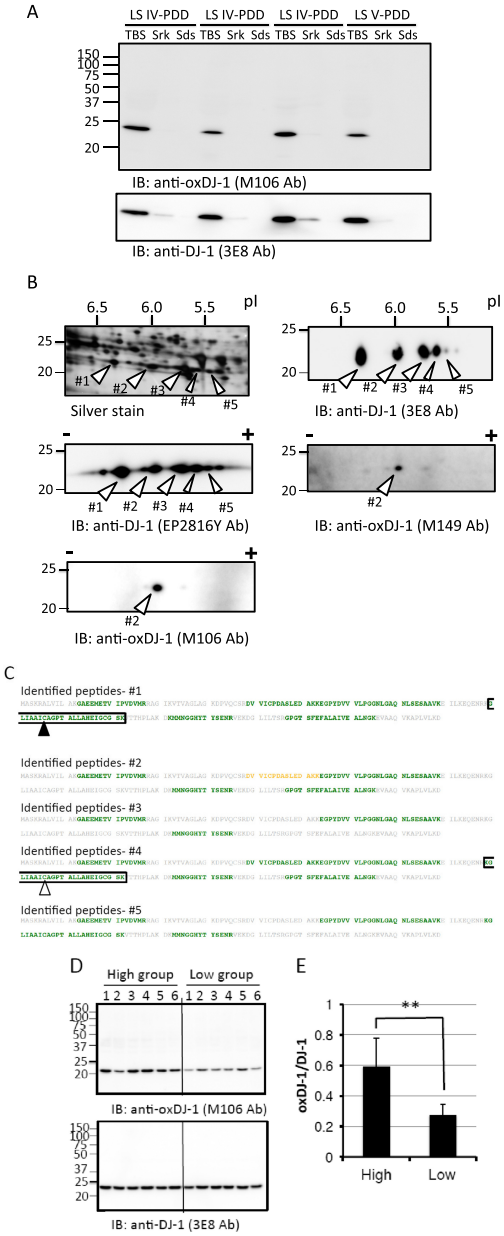

FIGURE 6. Western blot analyses of oxDJ-1 in frozen brain tissues from the medulla oblongata. **(A)** Tris-buffered saline-soluble, sarkosyl (Srk)–soluble, and SDS-soluble fractions were prepared from frozen brain tissues from the ION in which high levels of oxDJ-1 IR had been detected. Each fraction (100 μg of protein of TBS-soluble fraction, same fluid volume of Srk-soluble and SDS-soluble fractions) was subjected to Western blot analyses using the anti–DJ-1 and anti–oxDJ-1 mAbs. **(B)** Lysates (for Western blot analysis) from the TBS-soluble fraction of frozen brain tissues from the ION were separated by 2D-PAGE and subjected to silver staining (200 μg) and Western blot analysis (100 μg) using anti–oxDJ-1 (clones M149 and M106) and anti–DJ-1 (clones 3E8 and EP2816Y) mAbs. The identification number and calculated p*I* of each spot are as follows: native DJ-1, ID 1, p*I* of 6.3; oxDJ-1, ID 2, p*I* of 6.0; DJ-1 with unknown modification, ID 3, p*I* of 5.7; DJ-1 with unknown modification, ID 4, p*I* of 5.6; DJ-1 with unknown modification, ID 5, p*I* of 5.4. **(C)** Matrix-assisted laser desorption/ionization TOF MS analysis of DJ-1 spots in the TBS-soluble fractions of the ION. The stained spots corresponding to DJ-1 (ID 1–ID 5 in **B**) were subjected to in-gel digestion and analyzed by MALDI-TOF MS. Peptides containing Cys106-SH and Cys106-SO_3H are shown in black and white black arrowheads, respectively. Identified peptide sequences with confidence intervals greater than 95% are shown in green. The sequence indicated by yellow corresponds to confidence intervals higher than 50%. In this analysis, Cys106-SH was identified in spot 1 **(A)**, whereas Cys106-SO_3H was not identified in spot 2 **(B)**; Cys106-SO_2H was identified in spot 4 **(D)**. **(D)** Lysates (100 μg) from frozen brain tissues from the ION with high (n = 6) and low (n = 6) oxDJ-1 IR were separated by SDS-PAGE and subjected to Western blot analyses using oxDJ-1 (clone M106) and DJ-1 (clones 3E8) mAbs. **(E)** Quantitative analyses of oxDJ-1 levels between the high–oxDJ-1 IR group and the low–oxDJ-1 IR group. The relative densities of oxDJ-1 normalized to DJ-1 were calculated and presented as mean ± SD(n = 6). ** $p < 0.01$, Student t-test. IB, immunoblot; LS IV–PDD, dementia with LBs, transitional (limbic) form; LS V–PDD, dementia with LBs, neocortical form (diffuse LB disease).

oxDJ-1 IR was observed within the cell bodies of neurons, the nuclei of glial cells, and neuropil (Fig. 2J). The specificity of oxDJ-1 staining at high magnification was confirmed by the absence of IR in KO mice (Figs. 2K, L). DJ-1 staining at high magnification is also shown in Figure, Supplemental Digital Content 1, parts G–L, http://links.lww.com/NEN/A603. Oxidized DJ-1 IR staining of neuron processes was variable in the cortex, hippocampus, and SN. The distribution of oxDJ-1 IR in normal mouse brains is summarized in Table 2.

OxDJ-1 IR in Dopaminergic Nigral Neuronal Cells and Glial Cells of the Midbrain of Human Subjects

To assess the levels and distribution of oxDJ-1 in the progression of PD, we performed immunohistochemical studies, using mAbs against oxDJ-1, on human postmortem brain sections (including the midbrain, striatum, and medulla oblongata) from control and PD cases with different LB stages and PDD (Table 1). The distribution of oxDJ-1 IR in human brain sections is summarized in Table 2.

In the dopaminergic nigral neuronal cells of LB stage (LS) III–PD patients, obvious oxDJ-1 IR in cell bodies and neurites was observed using confocal microscopy (Fig. 3A). As in the oxDJ-1 IR observed in mice, marked oxDJ-1 IR staining of neuropil was observed in the SN of human subjects. The oxDJ-1 IR detected in cell bodies and neurites was abolished in the absence of the oxDJ-1 antibody (Fig. 3A). Double immunostaining showed that the portions labeled with anti–oxDJ-1 antibody and anti-phosphorylated α-synuclein antibody (indicative of LBs) colocalized (Figs. 3A, B). Oxidized DJ-1 IR was widely distributed throughout cell bodies and neurites of the SN; however, in the periphery of the SN, there was oxDJ-1 IR of neuron processes (Fig. 3C).

Results for 3,3-diaminobenzidine staining of the midbrain, using the oxDJ-1 mAb, are shown in Figure 3D and Figure, Supplemental Digital Content 2, http://links.lww.com/NEN/A604. Oxidized DJ-1 IR was prominent in the SN and red nucleus in LS III–PD patients; staining was not observed without the primary antibody (Fig. 3D). In the SN and red nucleus of control subjects (LS 0), oxDJ-1 IR was also observed. DJ-1 immunostaining using clones EP2816Y and 3E8 resulted in slight but significant staining of the SN and red nucleus (Fig. 3D). At high magnification, there was staining of cell bodies, neurites, and neuropil of neuromelanin-containing neurons in the SN using the oxDJ-1 mAb (Fig. 3E). In the periphery of the SN, there was oxDJ-1 IR of neuron processes (Fig. 3F). In the red nuclei, there was oxDJ-1 IR of glial cells (Fig. 3G). Absence of immunostaining was confirmed in secondary-antibody-only controls (Fig. 3H). Oxidized DJ-1 IR in the SN was compared in LS 0 to LS V–PDD cases (Figure, Supplemental Digital Content 2, http://links.lww.com/NEN/A604). It seemed that oxDJ-1 IR of the SN increased in LS II and LS III–PD cases and then decreased in LS IV– and LS V–PDD cases (Table 1; Figure, Supplemental Digital Content 2, http://links.lww.com/NEN/A604). Collectively, these observations suggest the formation of oxDJ-1 in dopaminergic nigral neuronal cells and the alteration of oxDJ-1 formation in the progression of PD.

OxDJ-1 IR in the Human Striatum

In the striatum of LS II patients, immunostaining for oxDJ-1 was evident in the putamen at low magnification; staining was not observed without the primary antibody (Fig. 4A). In the striatum of control subjects (LS 0), oxDJ-1 IR was also observed (Figure, Supplemental Digital Content 3, part A, http://links.lww.com/NEN/A605). In contrast, DJ-1 IR using mAbs EP2816Y and 3E8 resulted in staining of both the putamen and the internal capsule (Fig. 4A). At high magnification of the putamen, staining of glial cells with oxDJ-1 mAbs was evident (Figs. 4B, C). Oxidized DJ-1 IR was also observed in neuropil of the putamen. The relative degrees of oxDJ-1 IR in the striatum are summarized in Table 1. It seems that oxDJ-1 IR of the striatum correlated with that of the SN (Table 1). Astrocyte expression of oxDJ-1 in the striatum was confirmed using double immunostaining with anti–glial fibrillary acidic protein (Fig. 4D). The images clearly show positive staining of cell bodies and proximal processes of astrocytes. These results suggest that although oxDJ-1 is generated in both the astrocytes and the neurons of the striatum, astrocytes express oxDJ-1 more robustly in the striatum.

OxDJ-1 IR in the Human Medulla Oblongata

In the medulla oblongata of LS III–PD patients, oxDJ-1 IR was prominent in the inferior olivary nucleus (ION) at low magnification; obvious staining was not observed without the primary antibody (Fig. 5A). Oxidized DJ-1 IR was also observed in the ION of control subjects (LS 0) (Figure, Supplemental Digital Content 3, part B, http://links.lww.com/NEN/A605). Relative oxDJ-1 IR in the ION is summarized in Table 1. For DJ-1 immunostaining using clones EP2816Y and 3E8, there was also staining of the ION (Fig. 5A). At low magnification, there was slight oxDJ-1 IR observed in the dorsum of the medulla oblongata (Fig. 5A), including the vagus nerve dorsum nucleus (VNDN). At high magnification, marked staining was observed with the oxDJ-1 mAb in neuron cell bodies and neurites in the VNDN, one of the lesion sites in PD (Fig. 5B). Clear positive staining of neuronal cell bodies and surrounding glial cells was observed in the ION (Figs. 5C, D). There was also IR of neuropil in these areas. Absence of immunostaining was confirmed under control conditions (Fig. 5E). These results suggest the generation of oxDJ-1 in the VNDN and ION. Colocalization of oxDJ-1 and LBs in the VNDN was further examined. Double immunostaining at high magnification showed that portions labeled with anti–oxDJ-1 antibody and anti-phosphorylated α-synuclein antibody colocalized in the VNDN (Fig. 5F).

Biochemical Analyses of OxDJ-1 in the ION

The biochemical properties of oxDJ-1 in frozen brain samples were further investigated using the oxDJ-1–specific antibodies M106 and M149. Frozen brain tissues around the ION with high oxDJ-1 levels were homogenized, and TBS-soluble, sarkosyl-soluble, and SDS-soluble fractions were prepared. Proteins in these fractions were separated by SDS-PAGE and 2D-PAGE, and oxDJ-1 was detected using the oxDJ-1 antibody. Most of the oxDJ-1 was detected in the TBS-soluble fraction, migrating with an apparent molecular

mass of 21 kDa, corresponding to DJ-1 (Fig. 6A). As shown in Figure 6B, Western blot analysis of the TBS-soluble fraction separated by 2D-PAGE revealed several spots with the DJ-1 antibody (clones 3E8 and EP2816Y). The arrowheads in Figure 6B indicate the spots in which DJ-1 could be identified by liquid chromatography MS/MS analysis (Fig. 6C). In the oxDJ-1 blot, the major spot was identified as spot 2, corresponding to the theoretical p*I* of oxDJ-1 (Fig. 6B).

To further examine the correlation between immunostaining and Western blot analysis, we determined oxDJ-1 levels in the ION of frozen brain tissues based on Western blot analysis. Six sections with high and low oxDJ-1 IR in the ION were selected based on the intensity of 3,3-diaminobenzidine staining (Figure, Supplemental Digital Content 4, http://links.lww.com/NEN/A606); these frozen ION tissues were subjected to Western blot analysis using anti–oxDJ-1 antibody. Consistent with immunostaining, oxDJ-1 band intensity in the ION of the high–oxDJ-1 IR group was significantly higher than that in tissues from the low–oxDJ-1 IR group (Fig. 6D). Band intensities of the oxDJ-1 and DJ-1 blots were determined, and oxDJ-1–DJ-1 ratios were calculated. As shown in Figure 6E, there was a significant difference in the oxDJ-1–DJ-1 ratio between the high–oxDJ-1 IR group and the low–oxDJ-1 IR group.

DISCUSSION

Cys106 of DJ-1 is the cysteine residue most sensitive to oxidation. Several previous studies have demonstrated the important role of Cys106 in the biologic function of DJ-1 (3, 5, 6, 11), but the detailed distribution of oxDJ-1 in the human brain and the relationship of DJ-1 oxidation with the progression of PD have not been elucidated. Using oxDJ-1–specific antibodies, this study shows that oxDJ-1 is present in glial and neuronal cells of the human brain and that oxDJ-1 levels might change during the progression of LB-associated neurodegenerative diseases.

Oxidized DJ-1 IR was observed in cell bodies and neurites in dopaminergic nigral neurons of mice and humans (Figs. 2, 3). Previous studies have demonstrated the important role of DJ-1 in the synthesis of dopamine (28, 29). DJ-1 upregulates the transcription of tyrosine hydroxylase, the rate-limiting enzyme of dopamine synthesis, by inhibiting the sumoylation of pyrimidine tract binding protein–associated splicing factor (28). Furthermore, DJ-1 activates dopamine synthesis through interaction with dopamine biosynthetic enzymes, such as tyrosine hydroxylase and 4-dihydroxy-L-phenylalanine decarboxylase, in an oxidation-dependent manner (29). In a previous study, slight oxidative stress inducing DJ-1 oxidation to Cys106-SOH was found to upregulate dopamine synthesis, whereas extensive oxidative stress inducing DJ-1 oxidation to Cys106-SO_2H or Cys106-SO_3H was found not to upregulate dopamine production (29). In the present study, the presence of DJ-1 Cys106-SO_2H or Cys106-SO_3H was shown in normal SNs of humans and mice. Thus, we hypothesize that the regulation of dopamine synthesis via DJ-1 oxidation may occur under physiologic conditions. Notably, the maximal oxDJ-1 IR in the SN was observed in cases classified as LS II and LS III–PD (i.e. when LBs are present either with or without associated parkinsonism). Therefore, oxDJ-1 might be formed and thus decrease dopamine synthesis at the early stages of clinical disease. Western blot analysis of proteins separated using 2D-PAGE revealed that our oxDJ-1 mAbs mainly detected DJ-1 at spot 2 (Fig. 6B). We also observed that the more acidic DJ-1 at spots 3, 4, and 5 were not detected by Western blot analysis with the anti–oxDJ-1 mAbs. This result suggests that our oxDJ-1 mAbs do not react to a great extent with highly modified DJ-1. Oxidized DJ-1 IR in the SN might decrease in patients with LS IV– and LS V–PDD (Figure, Supplemental Digital Content 2, http://links.lww.com/NEN/A604; Table 1). In these later stages, the decrease in oxDJ-1 levels seems to reflect further modification of oxDJ-1, correlating with the decrease in dopaminergic cells in the SN.

DJ-1 is an important factor for defense against oxidative stress. Several studies have reported that DJ-1 is involved in the regulation of glutathione metabolism and in the gene expression of 2 uncoupling proteins (UCP4 and UCP5) (6, 30). DJ-1 can react with ROS such as H_2O_2; however, this reaction is not enzyme-catalyzed (3) and might be less efficient compared with other antioxidative enzymes, including glutathione peroxidase and catalase. Therefore, it is reasonable to consider that DJ-1 plays a role in antioxidative defense via oxidation of Cys106 of DJ-1 to regulate transcription factors rather than removing ROS via direct oxidation of Cys106. Recent evidence also suggests that DJ-1 acts as a sensor to alter gene expression levels that are involved in antioxidative defense systems in response to oxidative stress (11, 20). Therefore, oxDJ-1 IR may, at least in part, be hypothesized to reflect DJ-1 functions, via oxidation of Cys106, that detect and manage ROS-induced insults.

Obvious oxDJ-1 and DJ-1 IR was observed in neuropil in multiple sites of human and mouse brains. A previous study has reported the presence of DJ-1 IR in neuropil (17). It has recently been reported that DJ-1 is required for the normal expression of β-tubulin III, suggesting a possible role for DJ-1 in the regulation of microtubule dynamics (31). In addition, DJ-1 has been reported to act as a molecular chaperone to inhibit aggregation of microtubule-associated protein 1B (32). It has also been shown that DJ-1 acts as a redox-activated chaperone toward α-synuclein (12). The vital role of microtubules in axon guidance and outgrowth of neurites is also known (33). Collectively, it seems that DJ-1 in neuropil might play a role in the structure and function of microtubules in an oxidation-dependent manner.

In the present study, marked oxDJ-1 IR in cells with astrocyte morphology was observed in the striatum (Fig. 4). Glial cells were also immunostained with the oxDJ-1 mAb in other sites, including the cortex, striatum, SN, and red nucleus, and in the ION and VNDN. These results suggest the importance of DJ-1 in glial cells. Astrocytes are neuroprotective, and there is an inverse correlation between astrocyte number and dopaminergic cell loss (34). Astrocytes possess higher levels of antioxidant enzymes that protect neurons from oxidative stress, and previous studies have reported a high expression of DJ-1 in astrocytes and its importance for the astrocyte function of astrocytes (35, 36). It has recently been demonstrated that DJ-1 plays an important role in the neuroprotective effects of astrocytes (37). Therefore, glial

cells are considered to be important contributors to the prevention of oxidative stress in PD, and DJ-1 likely plays a significant role in the antioxidative function of astrocytes via oxidation of Cys106.

Interestingly, in addition to the marked oxDJ-1 IR in the SN, the red nucleus shows prominent oxDJ-1 IR. The red nucleus is involved in motor coordination; the red nucleus and the SN are subcortical centers of the extrapyramidal motor system. In addition, neurons in the ION showed prominent oxDJ-1 IR. The ION is associated with the cerebellum; therefore, neurons in this area are also involved in movement control and coordination. Although the physiologic and pathologic significance of oxDJ-1 in these sites is unclear at present, DJ-1 might function to protect neurons in the ION via Cys106 oxidation and contribute to movement control.

One limitation of the present study is that the selectivity of the oxDJ-1 antibodies against the Cys-SO_2H or Cys-SO_3H form of oxDJ-1 is unknown. The Cys106-SO_3H form was mainly detected by MALDI-TOF MS analysis; however, the Cys106-SO_2H residue in the digested peptide is easily oxidized to Cys106-SO_3H. Therefore, we cannot rule out the possibility that the prepared oxDJ-1 recombinant protein contains the Cys106-SO_2H isoform. The denaturing procedure may also affect the oxidation state of Cys106 because the tertiary structure of the Cys106-SO_2H isoform of oxDJ-1 prevents further oxidation from Cys106-SO_2H to Cys106-SO_3H. It would be useful to develop a method for distinguishing between the Cys-SO_2H and Cys-SO_3H forms of oxDJ-1 to understand the biologic function of different DJ-1 oxidation isoforms.

In conclusion, immunohistochemical and biochemical analyses using specific antibodies against oxDJ-1 indicate the presence of oxDJ-1 in neuronal and glial cells. In addition, a change in oxDJ-1 levels in the SN was suggested during PD progression. These observations suggest the significance of DJ-1 oxidation in the function of neuronal and glial cells, particularly in the regulation of dopamine synthesis in the SN. Our observations suggest the relevance of DJ-1 oxidation to homeostasis in multiple sites of the brain, including neuromelanin-containing neurons of the SN.

ACKNOWLEDGMENTS

We thank Rie Yasuda, Kozue Hirai, Shigeichi Shono, Kenichiro Jitta, and Maya Suetsugu for technical assistance.

REFERENCES

1. Lesage S, Brice A. Role of Mendelian genes in ''sporadic'' Parkinson's disease. Parkinsonism Relat Disord 2012;18(Suppl 1):S66–70
2. Bonifati V, Rizzu P, van Baren MJ, et al. Mutations in the *DJ-1* gene associated with autosomal recessive early-onset parkinsonism. Science 2003;299:256–59
3. Taira T, Saito Y, Niki T, et al. DJ-1 has a role in antioxidative stress to prevent cell death. EMBO Rep 2004;5:213–18
4. Inden M, Taira T, Kitamura Y, et al. PARK7 DJ-1 protects against degeneration of nigral dopaminergic neurons in Parkinson's disease rat model. Neurobiol Dis 2006;24:144–58
5. Wang Z, Liu J, Chen S, et al. DJ-1 modulates the expression of Cu/Zn–superoxide dismutase-1 through the Erk1/2–Elk1 pathway in neuroprotection. Ann Neurol 2011;70:591–99
6. Guzman JN, Sanchez-Padilla J, Wokosin D, et al. Oxidant stress evoked by pacemaking in dopaminergic neurons is attenuated by DJ-1. Nature 2010;468:696–700
7. Lotharius J, Brundin P. Pathogenesis of Parkinson's disease: Dopamine, vesicles and α-synuclein. Nat Rev Neurosci 2002;3:932–42
8. Sayre LM, Perry G, Smith MA. Oxidative stress and neurotoxicity. Chem Res Toxicol 2008;21:172–88
9. Kinumi T, Kimata J, Taira T, et al. Cysteine-106 of DJ-1 is the most sensitive cysteine residue to hydrogen peroxide–mediated oxidation in vivo in human umbilical vein endothelial cells. Biochem Biophys Res Commun 2004;317:722–28
10. Blackinton J, Lakshminarasimhan M, Thomas KJ, et al. Formation of a stabilized cysteine sulfinic acid is critical for the mitochondrial function of the parkinsonism protein DJ-1. J Biol Chem 2009;284:6476–85
11. Wilson MA. The role of cysteine oxidation in DJ-1 function and dysfunction. Antioxid Redox Signal 2011;15:111–22
12. Zhou W, Zhu M, Wilson MA, et al. The oxidation state of DJ-1 regulates its chaperone activity toward α-synuclein. J Mol Biol 2006;356:1036–48
13. Saito Y, Hamakubo T, Yoshida Y, et al. Preparation and application of monoclonal antibodies against oxidized DJ-1. Significant elevation of oxidized DJ-1 in erythrocytes of early-stage Parkinson disease patients. Neurosci Lett 2009;465:1–5
14. Akazawa YO, Saito Y, Hamakubo T, et al. Elevation of oxidized DJ-1 in the brain and erythrocytes of Parkinson disease model animals. Neurosci Lett 2010;483:201–5
15. Bandopadhyay R, Kingsbury AE, Cookson MR, et al. The expression of DJ-1 (PARK7) in normal human CNS and idiopathic Parkinson's disease. Brain 2004;127:420–30
16. Neumann M, Muller V, Gorner K, et al. Pathological properties of the Parkinson's disease–associated protein DJ-1 in α-synucleinopathies and tauopathies: Relevance for multiple system atrophy and Pick's disease. Acta Neuropathol 2004;107:489–96
17. Kumaran R, Kingsbury A, Coulter I, et al. DJ-1 (PARK7) is associated with 3R and 4R tau neuronal and glial inclusions in neurodegenerative disorders. Neurobiol Dis 2007;28:122–32
18. Rizzu P, Hinkle DA, Zhukareva V, et al. DJ-1 colocalizes with tau inclusions: A link between parkinsonism and dementia. Ann Neurol 2004;55:113–18
19. Choi J, Sullards MC, Olzmann JA, et al. Oxidative damage of DJ-1 is linked to sporadic Parkinson and Alzheimer diseases. J Biol Chem 2006;281:10816–24
20. Miyama A, Saito Y, Yamanaka K, et al. Oxidation of DJ-1 induced by 6-hydroxydopamine decreasing intracellular glutathione. PLoS One 2011;6:e27883
21. Saito Y, Nishio K, Ogawa Y, et al. Turning point in apoptosis/-necrosis induced by hydrogen peroxide. Free Radic Res 2006;40:619–30
22. Kim YC, Kitaura H, Iguchi-Ariga SM, et al. *DJ-1*, an oncogene and causative gene for familial Parkinson's disease, is essential for SV40 transformation in mouse fibroblasts through up-regulation of c-Myc. FEBS Lett 2010;584:3891–95
23. Saito Y, Ruberu NN, Sawabe M, et al. Lewy body–related α-synucleinopathy in aging. J Neuropathol Exp Neurol 2004;63:742–49
24. Hughes AJ, Daniel SE, Kilford L, et al. Accuracy of clinical diagnosis of idiopathic Parkinson's disease: A clinico-pathological study of 100 cases. J Neurol Neurosurg Psychiatry 1992;55:181–84
25. McKeith IG, Galasko D, Kosaka K, et al. Consensus guidelines for the clinical and pathologic diagnosis of dementia with Lewy bodies (DLB): Report of the Consortium on DLB International Workshop. Neurology 1996;47:1113–24
26. McKeith IG, Dickson DW, Lowe J, et al. Diagnosis and management of dementia with Lewy bodies: Third report of the DLB Consortium. Neurology 2005;65:1863–72
27. Miyasaka T, Watanabe A, Saito Y, et al. Visualization of newly deposited tau in neurofibrillary tangles and neuropil threads. J Neuropathol Exp Neurol 2005;64:665–74
28. Zhong N, Kim CY, Rizzu P, et al. DJ-1 transcriptionally up-regulates the human tyrosine hydroxylase by inhibiting the sumoylation of pyrimidine tract–binding protein–associated splicing factor. J Biol Chem 2006;281:20940–48
29. Ishikawa S, Taira T, Niki T, et al. Oxidative status of DJ-1–dependent activation of dopamine synthesis through interaction of tyrosine hydroxylase and 4-dihydroxy-ι-phenylalanine (ι-DOPA) decarboxylase with DJ-1. J Biol Chem 2009;284:28832–44

30. Zhou W, Freed CR. DJ-1 up-regulates glutathione synthesis during oxidative stress and inhibits A53T α-synuclein toxicity. J Biol Chem 2005; 280:43150–58
31. Sheng C, Heng X, Zhang G, et al. DJ-1 deficiency perturbs microtubule dynamics and impairs striatal neurite outgrowth. Neurobiol Aging 2013; 34:489–98
32. Wang Z, Zhang Y, Zhang S, et al. DJ-1 can inhibit microtubule associated protein 1 B formed aggregates. Mol Neurodeg 2011;6:38
33. Conde C, Caceres A. Microtubule assembly, organization and dynamics in axons and dendrites. Nat Rev Neurosci 2009, 10:319–32
34. Damier P, Hirsch EC, Zhang P, et al. Glutathione peroxidase, glial cells and Parkinson's disease. Neuroscience 1993;52:1–6
35. Mullett SJ, Hamilton RL, Hinkle DA. DJ-1 immunoreactivity in human brain astrocytes is dependent on infarct presence and infarct age. Neuropathology 2009;29:125–31
36. Larsen NJ, Ambrosi G, Mullett SJ, et al. DJ-1 knock-down impairs astrocyte mitochondrial function. Neuroscience 2011;196:251–64
37. Mullett SJ, Di Maio R, Greenamyre JT, et al. DJ-1 expression modulates astrocyte-mediated protection against neuronal oxidative stress. J Mol Neurosci 2013;49:507–11